Xiaoping Gao[1,*], Xiaori Yang[1], Danxi Li[1], Yonggui Li[2,**]

Experimental and Numerical Simulation of the Tensile Behaviour of a Biaxial Warp-knitted Composite

DOI: 10.5604/01.3001.0012.5164

[1] **Inner Mongolia University of Technology, College of Light Industry and Textile,** Hohhot, 010051, China
* e-mail: gaoxp@imut.edu.cn

[2] **Minjiang University, Fujian Key Laboratory of Novel Funcional Textile Fibres and Materials,** Fuzhou, Fujian, 350108 China
** e-mail: lygwxjd@sina.com

Abstract
In this paper a composite reinforced with biaxial warp-knitted fabric and epoxy resin was manufactured by applying vacuum assisted resin transfer moldings (VARTM). The quasi--static tensile behaviour was experimentally tested in 0° and 90° directions, respectively. A finite element model of biaxial warp-knitted composites was developed on a meso-scale. The tensile behaviour of the composites was numerical simulated and compared with the experimental results. It showed that there is an approximate agreement between experimental and numerical results. There are maximum errors sum of squares of 14.52% and 33.29%. The finite element model of biaxial warp-knitted composites has higher accuracy, which can be used to study the static and dynamic mechanical properties.

Key words: *biaxial warp-knitted composite, tensile behavior, finite element analysis.*

Introduction

Multi-axial warp-knitted composites are widely used in the aerospace and marine industries, as well as in wind turbine blades and other complex structural components due to their excellent strength and stiffness to weight ratio [1-4]. In multi-axial warp-knitted fabrics, since the fiber bundles are not interlaced with each other, the laid fiber bundles are aligned in a straight line so that the fiber bundles can exhibit maximum tensile strength. They are manufactured from multiple layers of straight fiber bundles with different orientations stitched together by the warp knitting procedure, greatly improving the economic benefits [5, 6].This makes them attractive materials for use in high-performance composite parts [7, 8]. With the rapid development of computer technology, the application of finite element simulation analysis of composite materials' mechanical, thermal conductivity and electromagnetic performance has become one of the most effective methods to ensure accurate, efficient and flexible analysis, greatly reducing the cost of experiment analysis. Abaqus is more advanced commercial software in the field of FEA, with a strong advantage in simple linear simulation and nonlinear correlation problem analysis.

Gao, et al. [9] tested the tensile-tensile fatigue behaviour of a multi-axial warp-knitted reinforced composite. Post-fatigue failure was attributed to debonding between the fiber and matrix after 1/3N and 2/3N at the 75% stress level. Wang, et al [10] studied the strength and damage of uniaxial composites, matrix fracture, fiber/matrix interface damage and fiber damage with numerical simulation. The results finally showed that the damage was consistent with the experimental results from the fiber fracture to matrix fracture. Mramesh, et al. [11] evaluated the tensile properties, flexural properties and impact properties of hybrid composites reinforced with kenaf and glass fibers by means of finite element analysis and experimental testing. Yang, et al. [12] compared the experimental results with those simulated for 3D orthogonal woven composites. The results showed that the maximum differences are 3.23% and 7.94% in 0° and 90° directions, and the model could be used to simulate the tensile properties of 3DOWC. Xu, et al. [13] studied the uni-axial tensile behaviour of metallic warp-knitted fabric by FEA. The simulation was in good agreement with the experimental tensile process. Wan, et al. [14] analysed the damage behaviors of biaxial multi-layer warp-knitted composite materials subjected to quasi-static and high strain rate compressions using the multi-scale method. Jiang, et al. [15] researched the tensile and ballistic penetration damage characterisations of a 2D triaxially braided composite by multi-scale finite element analysis. The results showed that the locations of stress propagation, the stress distribution and progressive failure behaviour in the composites could be clearly shown in the finite element model. The finite element model of a plain weave composite was developed in [16], where the yarns developed, constituting unit cells, were considered as elastomers and transversely isotropic, and the matrix was considered as isotropic. Chao, et al. [17] conducted

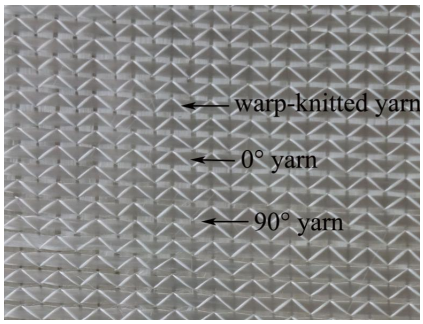

Figure 1. *Photograph of biaxial warp-knitted fabric.*

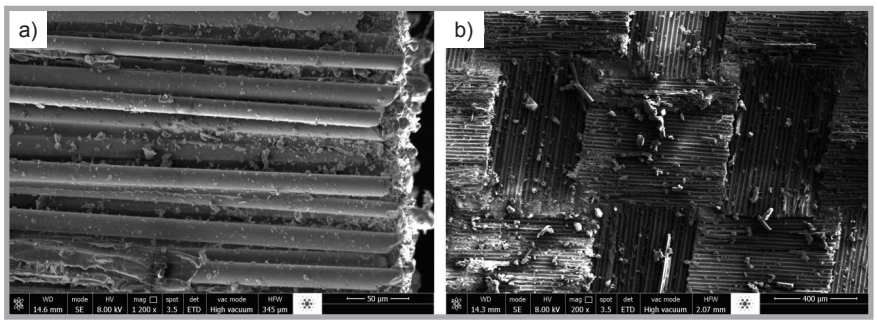

Figure 2. *SEM photographs of biaxial warp-knitted composites before tensile tests: a) surface of fibers, b) surface of fabric.*

a meso-scale finite element analysis of the mechanical behaviour of 3D braided composites subjected to biaxial tensile loadings. It was found that their findings may be a new reference for future investigations on the mechanical behaviour of other fiber composites. Thompson, et al. [18] investigated the stress field in the inter-layer of laminates under axial loading using the finite element method. Whitcomb, et al. [19] proposed an iterative holistic/local finite element analysis method. The basic idea is based on an overall model of the displacement and load as a local region analysis of the boundary conditions. The finite element method has been found to be one of the most powerful tools in analysing stress variation and computing the independent variation of stress with time [20]. Nowadays more and more researches are concerning on finite element analysis, which is high-tech as well as highly efficient and accurate. However, its applicability to biaxial warp-knitted glass fabric composites is restricted.

In this paper, the quasi-static tensile properties of biaxial glass fiber/epoxy composites manufactured by applying VARTM were tested in 0° and 90° directions. A three-dimensional model of biaxial warp-knitted fabric on a meso-scale was established based on ABAQUS software. The tensile behavior of biaxial warp-knitted composites in 0° and 90° directions were numerically simulated in Abaqus software, which were compared with the experimental results. The FE model verified could be used to analyse the tensile process and damage mechanism of biaxial warp-knitted fabric composites.

Materials

Biaxial warp-knitted fabric is composed of three systems of yarns, including warp, weft and warp-knitted yarns, which are bundled together in a warp-knitted structure [21]. The properties and photograph of biaxial warp-knitted fabric are shown in ***Table 1*** and ***Figure 1***.

Specimen preparation

The stacking sequence of the biaxial [0/90] laminates were (0/90, 0/90, 0/90, 0/90), which were laid onto the molding. A solution composed of 100 parts mass of epoxy resin (E-2511-1A) and 30 parts mass of curing agent (2511-1BT) was used for infusion at a vacuum pressure of -0.095 MPa. The flow of resin was controlled with the help of a peristaltic pump in such a way that it was allowed to flow in the distribution medium for some distance, and then the resin inlet was shut off to enable the resin to flow through the thickness. This cycle was repeated until the whole panel was soaked in resin. During injection, a vacuum of -0.095 MPa was applied in the cavity. After injection, the mould was transferred to a furnace maintained at 80 °C for 8 h for fast curing. The composite plate was then demoulded. Specimens were cut into narrow strips of 250 mm (length) × 25 mm (width) × 1 mm (thickness) according to ASTM D3039/3039M-14. In order to reduce damage to the sample in the clamping area and transfer the tensile load better from the clamping area, three-millimeter-thick composite end tabs with dimensions of 50 × 25 mm were glued onto the samples to minimise localised damage and to provide better load transfer from the grips to the specimens, respectively. The test speed was 2 mm/min, and the strain was continuously measured with an extensometer, where the gauge length between the top and bottom grip was set as 150 mm. A minimum of five samples were tested in each direction for each composite type. The fiber volume fraction of the composite specimen was obtained by applying igniting methods according to Standard GB/T 2577-2005. The specimen was burned in a muffle at a temperature of 450~650 °C and the epoxy evaporated. The fiber volume fraction was calculated by weighing the specimen and residue. The tensile behaviour of the biaxial warp-knitted composite is shown in ***Table 2***, and SEM photographs of the fiber surface and fractured sample before and after tensile tests are shown in ***Figures 2*** and ***3***.

The SEM photographs in ***Figure 2*** show that the fiber surface is smooth and neatly arranged, and that the interface between the resin and glass fiber is better bonded. Fiber debonding occurs after fracture, and fibers of varied length will be pulled out. ***Figure 3.a*** shows that the fiber fracture section is uneven and that the

Table 1. *Structure of biaxial warp-knitted fabric.*

Direction	Fiber bundle, μm	Thickness, mm	Mass, g/m²	Density, number/cm	Pile yarn, tex
Warp	15.00	0.700	1201	27.00	2400
Weft				22.00	1500

Tabele 2. *Biaxial warp-knitted composite tensile performance parameters.*

Specimen	Loading direction	Tensile strength, MPa	Tensile modulus, GPa	Fiber volume fraction, %	Normalised strength, MPa	Normalised modulus, GPa
Biaxial warp knitted composite	0°	153	3.47	51.2	134	3.05
	90°	78.6	4.99		69.1	4.38

fibers are ductile fractured. As shown in ***Figure 3.d***, it can be ascertained that the fiber is wrapped all around by the resin in the fracture section.

Fiber volume fraction calculation

The fiber volume fraction of the biaxial warp-knitted composite was calculated according to ***Equation (1)***. Average values of the mass and volume of composite samples before and after burning are shown in ***Table 3***.

The fiber volume fraction is V_f:

$$V_f = \frac{\rho_m W_f}{\rho_f W_m + \rho_m W_f} \times 100\% \qquad (1)$$

Where, ρ_m is the matrix density (g/cm^3), ρ_f is the glass fiber density (g/cm^3), W_m is the matrix quality (g), and W_f is the glass fiber quality (g).

Finite element model

In the finite element model of biaxial warp-knitted fabric, the warp and weft yarn were assumed as follows: (1) The yarn has a rectangular cross section; (2) the yarn is arranged evenly, and there is a certain distance to fill the matrix; (3) the yarn contacts directly with the matrix and there is no relative slippage.

The biaxial warp-knitted composites were combined with the resin very well in each layer. The role of the warp yarn was attributed to the resin, and the two parts were equivalent to a unidirectional composite. Therefore the model could be simplified as warp yarn, weft yarn and resin matrix. The matrix was assumed as isotropic material and the yarns considered as transversely isotropic.

Material parameters and damage criteria

Mechanical properties of the resin are shown as ***Table 4***. Mechanical properties of the glass fiber tows in 0° and 90° directions are shown as ***Table 5***, where subscripts 11 & 22 represent the axis direction of the coordinate system, subscripts 12, 13 & 23 – planes. X_T, X_C, Y_T & Y_C, and SS denote the tensile strength in the X direction, the compressive strength in the X direction, the tensile strength in the Y direction, the compressive strength in the Y direction, and the in-plane shear strength, respectively.

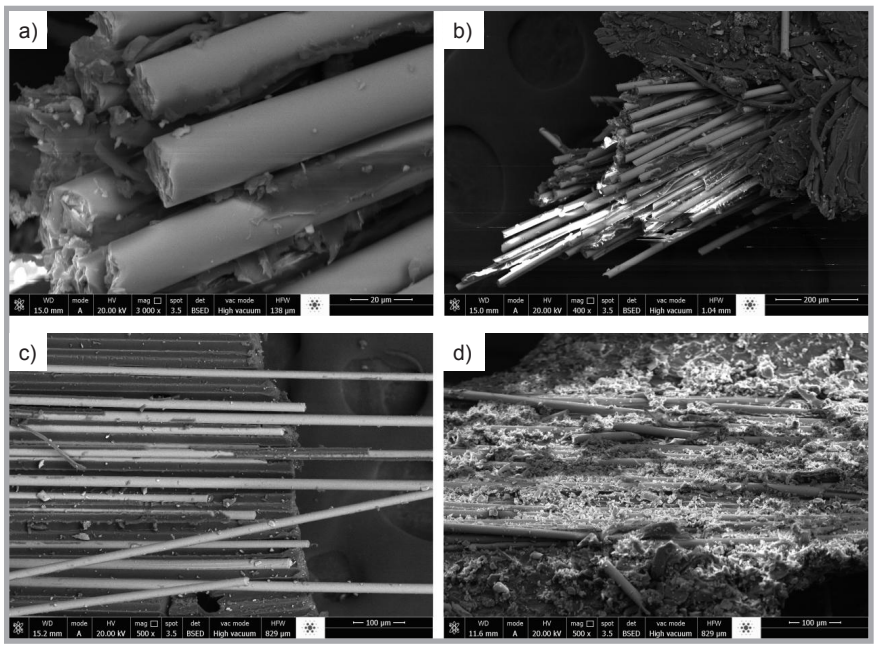

Figure 3. *SEM photographs of biaxial warp-knitted composites after tensile tests: a) fibre fracture morphology, b) fibre fracture in 0° direction, c) fibre fracture in 90° direction, d) fracture morphology on fabric surface.*

In order to simplify the modeling, the effect of the warp yarn on the composite material is equivalent to that of the matrix on the composite, i.e. the effect of the warp yarn is taken into account by strengthening the effect of the matrix on the composite. It was possible to obtain the mechanical properties of the equivalent "matrix" through the combination of the warp yarn, matrix volume ratio and its corresponding mechanical behaviour. Based on equations, the stiffness and intensity of the equivalent "matrix" were calculated using V_m and V_f, which are 43.4% and 56.6%, respectively, as shown in ***Tables 6*** and ***7***. The stiffness and strength of the equivalent "matrix" in ***Tables 6*** and ***7*** are cal-

Table 3. *Mass and volume of the sample before and after burning.*

Specimen	Volume, cm^3	Mass, g	Before burning (sample + crucible), g	After burning (sample + crucible), g
Biaxial warp-knitted composite	3.530	6.410	23.87	25.86

Table 4. *Mechanical properties of epoxy.*

Material	E, MPa	G, GPa	υ	X_T, MPa	X_C, MPa	S_S, MPa
Epoxy	3.20	1.25	0.25	80.0	150	160

Table 5. *Mechanical properties of fiber tows.*

Material	Density, g/cm^3	Elastic modulus, MPa	Break strength, MPa	Elongation at break, %	Shear modulus, GPa	Poisson's ratio, υ
0° direction yarn	2.560	30.00	1481	2.700	28.58	0.240
90° direction yarn	2.560	26.20	1566	2.700	28.58	0.240

Table 6. *Stiffness of equivalent "matrix".*

E_{11}, GPa	E_{22}, GPa	G_{12}, GPa	G_{13}, GPa	G_{23}, GPa	υ_{12}	υ_{23}	υ_{13}
3.40	2.36	0.07	0.07	0.05	0.23	0.22	0.23

Table 7. *Strength of equivalent "matrix".*

X_T, MPa	X_C, MPa	Y_T, MPa	Y_C, MPa	S_{S12}, MPa	S_{S23}, MPa
221.91	336.54	189.72	246.48	222.52	246.33

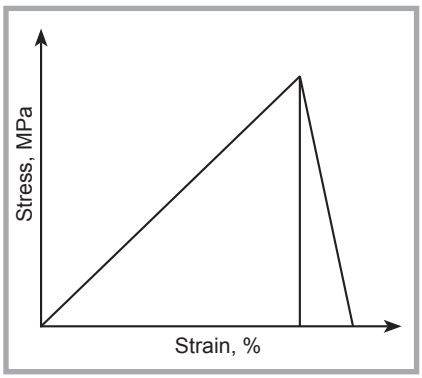

Figure 4. *Warp and weft yarn system fracture model.*

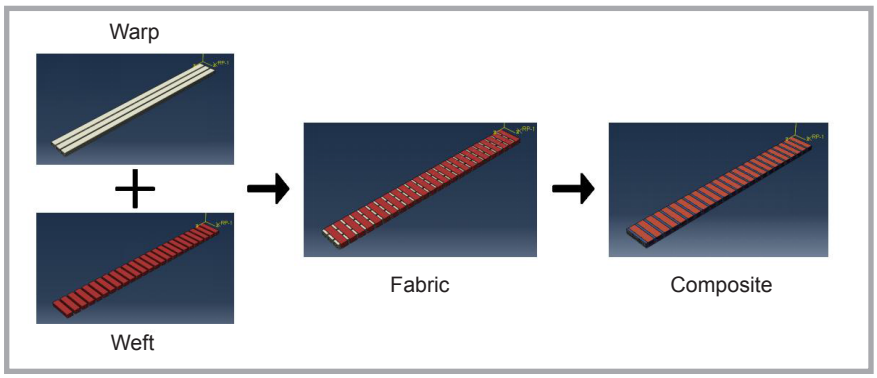

Figure 5. *Biaxial warp-knitted composite 3D solid model.*

culated according to ***Equations (2)***, ***(3)***, ***(4)*** and ***(16)***.

$$E_{11} = E_f V_f + E_m V_m \quad (2)$$

$$E_{22} = \frac{E_{f22} E_m}{V_f E_m + V_m E_{f22}} \quad (3)$$

$$\nu_{12} = V_f \cdot \nu_f + V_m \cdot \nu_m \quad (4)$$

$$\nu_{13} = V_f \nu_{f12} + V_m \nu_m \quad (5)$$

$$\nu_{23} = V_f \nu_{f22} + V_m \nu_m \quad (6)$$

$$G_{12} = \frac{G_{f12} G_m}{V_f G_m + V_m G_{f12}} \quad (7)$$

$$G_{13} = \frac{G_{f13} G_m}{V_f G_m + V_m G_{f13}} \quad (8)$$

$$G_{23} = \frac{G_{f23} G_m}{V_f G_m + V_m G_{f23}} \quad (9)$$

$$(\sigma_{11}^T)_{ult} = (\sigma_{f11}^T)_{ult} V_f + (\varepsilon_{f11}^T)_{ult} E_m (1 - V_f) \quad (10)$$

$$(\sigma_{11}^C)_{ult} = (\sigma_m^C)_{ult} (V_m + \frac{E_{f11} V_f}{E_m}) \quad (11)$$

$$(\sigma_{22}^T)_{ult} = [V_f \frac{E_m}{E_{f22}} + V_m] E_{22} (\varepsilon_{m22}^T)_{} \quad (12)$$

$$(\sigma_{22}^C)_{ult} = [V_f \frac{E_m}{E_{f22}} + V_m] E_{22} (\varepsilon_{m22}^C)_{ult} \quad (13)$$

$$(\tau_{12})_{ult} = G_{12} \cdot [V_f \frac{G_m}{G_f} + V_m] (\gamma_{12})_{mult} \quad (14)$$

$$(\tau_{13})_{ult} = G_{13} \cdot [V_f \frac{G_m}{G_{f13}} + V_m] (\gamma_{13})_{mult} \quad (15)$$

$$(\tau_{23})_{ult} = G_{23} \cdot [V_f \frac{G_m}{G_{f23}} + V_m] (\gamma_{23})_{mult} \quad (16)$$

Where E is Young's modulus, V is the volume fraction, ν is Poisson's ratio, τ is the shear stress, δ is the normal stress, γ is the shear strain, and G the shear modulus.

The stress-strain constitutive of the warp and weft yarn system is nonlinear, assuming that the material can withstand a certain force after reaching the maximum tensile strength and that the crack can be used to control the crack propagation in this process in order to allow the calculation to converge. The maximum principal stress fracture model is used to break the warp and weft yarn system, as shown in ***Figure 4***.

Unit cell model

To save computing time, only a 1/4 part of the composite material with a size of 125 mm × 12.5 mm × 2.8 mm was developed in ABAQUS.

In the fabric, the warp yarn has a length of 4.2 mm, consisting of a variety of material entity units, with a warp width of 4.2 mm, thickness of 0.45 mm and spacing of 0.8 mm, and with a weft width of 3.8 mm, thickness of 0.25 mm and spacing of 1.2 mm through the creation of parts ordered. The porosity of the material is 6.26%. A FE model of the warp-knitted composite is shown in ***Figure 5***.

Contact definition and boundary conditions

The biaxial warp-knitted composite is composed of warp yarn, weft yarn and matrix. In order to separate each component, the "tie" constraint was used to bind the warp yarn, weft yarn and matrix, and the "general" was used to constrain the inter-layer of the yarn during analysis.

An initial constraint is applied at one end of the model with three translational displacements of the main restraining end (Ux = Uy = Uz = 0), and a reference point is established at the other end of the model.

Meshing

When the grid size is small enough, with an approximate value of 3 mm, the calculation results are relatively stable. In this paper the mesh size is 3 mm and the element type is a three-dimensional solid hexahedral eight-node (C3D8R) linear reduction integral unit. The model meshing is shown in ***Figure 6***.

Simulation results and experiment verification

Damage fracture morphology

Stress distributions at different strain levels in 0° and 90° directions are shown in ***Figures 7*** and ***8***. ***Figure 7*** shows the damage fracture morphology at 8% strain in the 0° direction. The most serious fracture damage occurred in the force direction parallel to the warp yarn, which the red colour indicates. Due to the effect of the transverse weft and matrix, the fracture of the composites is caused by cracks which do not penetrate the whole section; however, the interval is scattered mainly because of the different mechanical properties of the materials.

Figure 8 shows the damage fracture morphology at 5% strain in the 90° direction. It can be concluded that the damage morphologies are located mainly in the 90° direction and that the yarns in the 0° direction and matrix are hardly broken.

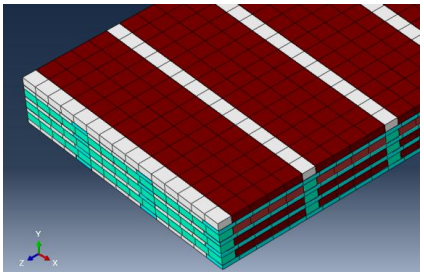

Figure 6. *Meshing.*

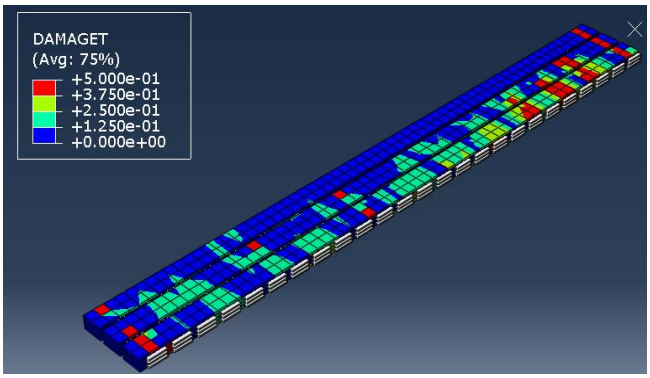

Figure 7. *Damage fracture morphology at 8% strain in 0° direction.*

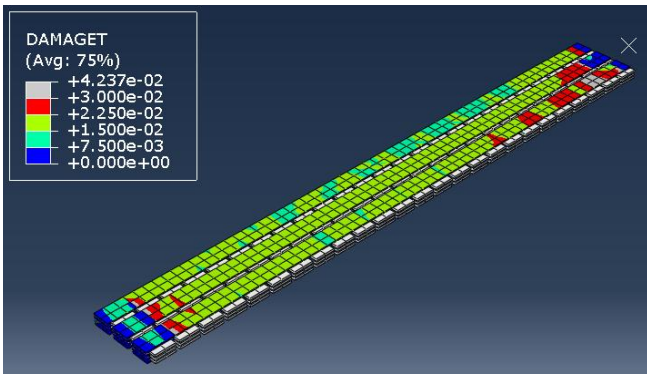

Figure 8. *Damage fracture morphology at 5% strain in 90° direction.*

When the specimen is stretched in the 90° direction, the load is afforded mainly by the weft yarn and matrix. Since the yarn in the 0° direction has a linearity of 2400 tex and the yarn in the 90° direction has only 1500 tex, it can be concluded that the stress tensors in the 0° direction are higher than that in 90° direction.

Results and discussion

The nominal stress-strain curve obtained from numerical simulation will be transformed into a real stress-strain curve process, i.e. curve $\overline{\sigma}-\eta$ is converted into curve $\sigma-\varepsilon$. The conversion formula is as follows:

$$\sigma = \overline{\sigma}e^{\varepsilon} \tag{17}$$

$$\varepsilon = \mathrm{Ln}(1+\eta) \tag{18}$$

Where $\overline{\sigma}$ is the engineering stress, η is the engineering strain, σ is the real stress, and ε is the real strain.

A comparison between stress-strain curves of the FEA simulation and experimental results is shown in ***Figure 9***. It is obvious from ***Figure 9*** that there are good agreements between experimental and numerical results in 0° and 90° directions. The maximum errors sum of squares for experimental results in 0° and 90° directions are 14.52% and 33.29% respectively. The slight deviation between experimental and numerical results was attributed to fact that the actual fiber distribution was not precisely modelled in the model. Moreover the slight deviation could be explained as the continuous nature of the model could not include the discontinuous and non-uniform microstructure of the material. It could also be explained by the effect of other factors, such as the neglecting of the contact between yarns and the influences of few internal pores and impurities. Therefore the finite element model could be used to predict other mechanical performance.

Conclusion

In this paper, the tensile behaviour of a biaxial warp-knitted composite on a meso-scale was studied. An FE model was developed in ABAQUS software to characterise the tensile behaviour of the biaxial warp-knitted composite. A composite specimen was also subjected to tensile tests in 0° and 90° directions, respectively. The experimental results were compared with finite element simulation data. There are maximum errors sum of squares of 14.52% and 33.29% in 0° and 90° directions respectively. It was found that there are approximate agreements, which proves the validity of the FE model. Therefore the FE model, which has advantages of lower time and economic costing, could be used to precisely predict the mechanical properties of other axial composites.

Acknowledgements

This work was supported by The National Natural Science Foundation of China (Grant Nos. 11462016, 51765051), The Natural Science Foundation of Inner Mongolia under grant No.2017MS0102, Scientific Research Innovation Funds for Postgraduates of Inner Mongolia (Grant No. S20171012809), and

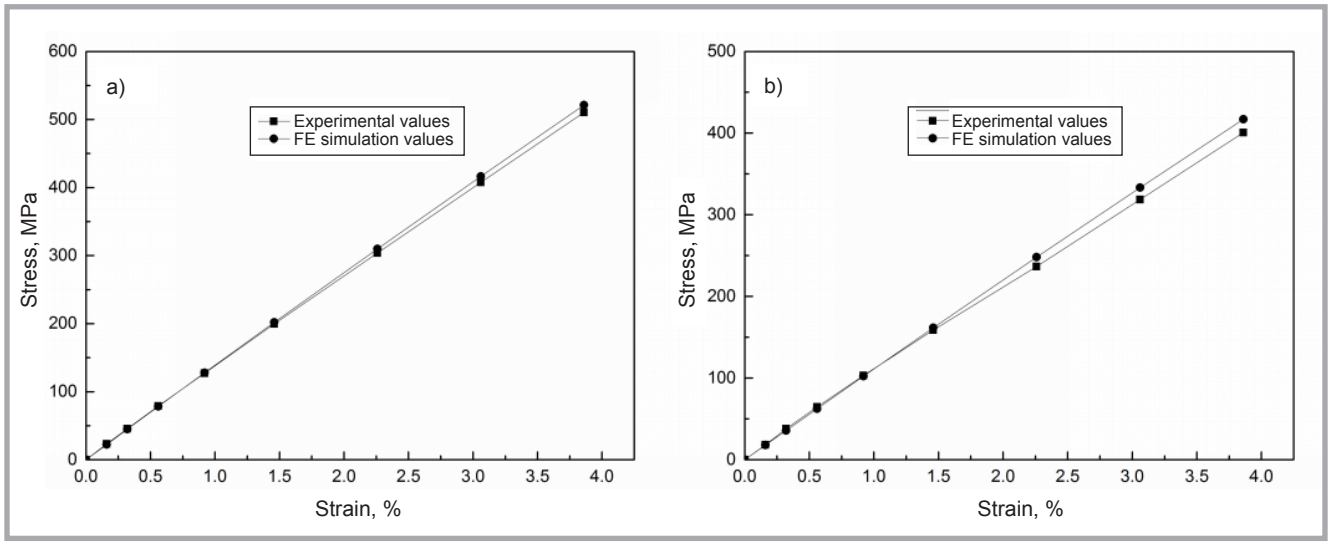

Figure 9. *FE results vs. experimental results: a) 0° direction, b) 90° direction.*

the Open Project Program of Fujian Key Laboratory of Novel Functional Textile Fibers and Materials, Minjiang University, China (No. KLTFM1807).

References

1. Mishnaevsky L, Brøndsted P, Nijssen R, et al. Materials of large wind turbine blades: recent results in testing and modeling. *Wind Energy* 2012; 15(1): 83-97.
2. Lee Y, Jhan Y, Chung C. Fluid-structure interaction of FRP wind turbine blades under aerodynamic effect. *Composites Part B: Engineering* 2012; 43(5): 2180-2191.
3. Wu Z Y, Tie L. The Application of Multi-Axial Warp Knitted Fabrics in Wind Turbine Blade. *Advanced Materials Research*. 2011; 95-297: 46-50.
4. Xu L, Jin C Z, Ha S K. Ultimate strength prediction of braided textile composites using a multi-scale approach. *Journal of Composite Materials*, 2014, 49(4): 477-494.
5. Loendersloot R, Lomov SV, Akkerman R, et al. Carbon composites based on multiaxial multiply stitched preforms. Part V: geometry of sheared biaxial fabrics. *Composites Part A: Applied Science and Manufacturing* 2006, 37(1): 103-113.
6. Lomov SV, Belov EB, Bischoff T, et al. Carbon composites based on multiaxial multiply stitched preforms. Part 1. Geometry of the preform. *Composites Part A: Applied Science and Manufacturing* 2002; 33(9): 1171-1183.
7. Vallons K, Lomov SV, Verpoest I. Fatigue and post-fatigue behaviour of carbon/epoxy non-crimp fabric composites. *Composites Part A: Applied Science and Manufacturing* 2009; 40(3): 251-259.
8. Wiśniewski J. Design of Lightweight Composite Disks Reinforced with Continuous Fibres. *FIBRES & TEXTILES in Eastern Europe* 2016; 24, 4(118): 74-79. DOI: 10.5604/12303666.1201134
9. Gao X, Tao N, Chen S, et al. Tensile-tensile Fatigue Behavior of Multi-axial Warp-knitted Reinforced Composite. *FIBRES & TEXTILES in Eastern Europe* 2018; 26, 1(127): 73-80. DOI: 10.5604/01.3001.0010.7800.
10. Wang H W, Zhou H W, Mishnaevsky L, et al. Single fibre and multifibre unit cell analysis of strength and cracking of unidirectional composites. *Computational Materials Science* 2009; 46(4): 810-820.
11. Ramesh M, Nijanthan S. Mechanical property analysis of kenaf–glass fibre reinforced polymer composites using finite element analysis. *Bull. Mater. Sci.* 2016; 39(1): 147-157.
12. Yang X, Gao X, Ma Y. Numerical Simulation of Tensile Behavior of 3D Orthogonal Woven Composites. *Fibers and Polymers* 2018; 19(3): 641-647.
13. Xu H, Jiang J, Cheng N, et al. Finite Element Modeling for the Uni-Axial Tensile Behaviour of Metallic Warp-Knitted Fabric. *FIBRES & TEXTILES in Eastern Europe*, 2018, 26, 2(128): 49-54. DOI: 10.5604/01.3001.0011.5738.
14. Wan Y, Sun B, Gu B. Multi-scale structure finite element analyses of damage behaviors of multi-axial warp-knitted composite materials subjected to quasi-static and high strain rate compressions. *The Journal of The Textile Institute* 2015; 107(7): 879-904.
15. Jiang H, Ren Y, Zhang S, et al. Multi-scale finite element analysis for tension and ballistic penetration damage characterizations of 2D triaxially braided composite. *Journal of Materials Science* 2018; 53(14): 10071-10094.
16. Glaessgen E H, Pastore C M, Griffin O H, et al. Geometrical and finite element modelling of textile composites. *Composites Part B: Engineering* 1996; 27(1): 43-50.
17. Zhang C, Curiel-Sosa J L, Bui T Q. Meso-Scale Finite Element Analysis of Mechanical Behavior of 3D Braided Composites Subjected to Biaxial Tension Loadings. *Applied Composite Materials* 2018:1-19.
18. Muheim D, Griffin O H. Verification of a 2-D to 3-D Global/Local Finite Element MEthod for Symmetric Laminates. *Journal of Reinforced Plastics and Composites* 1992; 11(8): 910-931.
19. Whitcomb Jd. Iterative Global/Local Finite Element Analysis. *Computers & Strucrures* 1991; 40(4): 1027-1031.
20. Gao X, Wang L. Finite Element Modelling for Tensile Behaviour of Thermally Bonded Nonwoven Fabric. *Autex Research Journal* 2015; 15(1): 48-53.
21. Li C, Wang J, Xue Z, et al. Research on Large Wind Turbine Blades Modeling Based on ANSYS. *Fiber Reinforced Plastics/Composites* 2009; (02): 52-55.

Received 15.11.2017 ***Reviewed 11.06.2018***

INSTITUTE OF BIOPOLYMERS AND CHEMICAL FIBRES

LABORATORY OF METROLOGY

IBWCh

Contact: Beata Pałys M.Sc. Eng.
ul. M. Skłodowskiej-Curie 19/27, 90-570 Łódź, Poland
tel. (+48 42) 638 03 41, e-mail: metrologia@ibwch.lodz.pl

AB 388

The **Laboratory** is active in testing fibres, yarns, textiles and medical products. The usability and physico-mechanical properties of textiles and medical products are tested in accordance with European EN, International ISO and Polish PN standards.

Tests within the accreditation procedure:
- linear density of fibres and yarns, mass per unit area using small samples, elasticity of yarns, breaking force and elongation of fibres, yarns and medical products, loop tenacity of fibres and yarns, bending length and specific flexural rigidity of textile and medical products

Other tests:
- **for fibres:** diameter of fibres, staple length and its distribution of fibres, linear shrinkage of fibres, elasticity and initial modulus of drawn fibres, crimp index, tenacity
- **for yarn:** yarn twist, contractility of multifilament yarns, tenacity,
- **for textiles:** mass per unit area using small samples, thickness
- **for films:** thickness-mechanical scanning method, mechanical properties under static tension
- **for medical products:** determination of the compressive strength of skull bones, determination of breaking strength and elongation at break, suture retention strength of medical products, perforation strength and dislocation at perforation

The Laboratory of Metrology carries out analyses for:
- research and development work, consultancy and expertise

Main equipment:
- Instron tensile testing machines, electrical capacitance tester for the determination of linear density unevenness – Uster type C, lanameter